Automatic Cerebral Microbleeds Detection from MR Images via Independent Subspace Analysis Based Hierarchical Features

Qi Dou, Hao Chen, Lequan Yu, Lin Shi, Defeng Wang, Vincent CT Mok and Pheng Ann Heng

***Abstract*— With the development of susceptibility weighted imaging (SWI) technology, cerebral microbleed (CMB) detection is increasingly essential in cerebrovascular diseases diagnosis and cognitive impairment assessment. Clinical CMB detection is based on manual rating which is subjective and time-consuming with limited reproducibility. In this paper, we propose a computer-aided system for automatic detection of CMBs from brain SWI images. Our approach detects the CMBs within three stages: (i) candidates screening based on intensity values (ii) compact 3D hierarchical features extraction via a stacked convolutional Independent Subspace Analysis (ISA) network (iii) false positive candidates removal with a support vector machine (SVM) classifier based on the learned representation features from ISA. Experimental results on 19 subjects (161 CMBs) achieve a high sensitivity of 89.44% with an average of 7.7 and 0.9 false positives per subject and per CMB, respectively, which validate the efficacy of our approach.**

***Index Terms*— Cerebral microbleed, brain SWI, feature representation, computer aided diagnosis**

I. Introduction

Cerebral microbleeds (CMBs) are perivascular collection of hemosiderin deposits in the brain. They can be visualized as rounded lesions of small size and low intensity in susceptibility weighted imaging (SWI) scans [1]. Clinically, CMBs have served as the biomarker for radiologic diagnosis of vessel diseases such as cerebral amyloid angiopathy. Detecting the existence of CMBs can also help to predict the future risk of symptomatic intracerebral hemorrhaging. Additionally, recent years of clinical studies showed that CMBs may have a direct effect on the neurological function and lead to cognitive impairment such as dementia [2].

The clinical CMB labeling is based on visual inspection and manual identification [3], which can be laborious, time-consuming, and subjective with limited reproducibility. Automatic computer-aided detection systems are therefore valuable alternatives which would help to improve the efficiency and reliability of the radiologic examination. However, automatic detection is challenging due to the small size (with a maximum diameter of 5 to 10 *mm*) and unpredictable distribution of CMBs [1]. Furthermore, there exist various

The work described in this paper was supported by the following grants from the Research Grants Council of the Hong Kong Special Administrative Region (Project No. CUHK 412412 and CUHK 14202514).

Q. Dou (email: qdou@cse.cuhk.edu.hk), H. Chen and P. A. Heng are with the Department of Computer Science and Engineering, The Chinese University of Hong Kong, Hong Kong. L. Yu is with the Department of Computer Science and Engineering, The Chinese University of Hong Kong, Hong Kong and the Department of Computer Science and Technology, Zhejiang University, China. L. Shi and V. Mok are with the Department of Medicine and Therapeutics, The Chinese University of Hong Kong, Hong Kong. D. Wang is with the Department of Imaging and Interventional Radiology, The Chinese University of Hong Kong, Hong Kong.

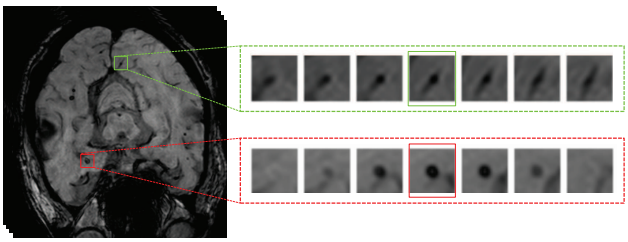

Fig. 1. Anatomical structure of true CMBs and CMB mimics in continuous slices. (Red rectangle and green rectangle denote true CMB and CMB mimic, respectively.)

CMB mimics (e.g., vein tissues, clacium and iron deposits) carrying similar appearance as CMBs in SWI scans, which confounds the detection procedure and increases the rate of false positive (FP) results [4].

In the last decade, several computer-aided methods have been developed for CMB detection by taking advantage of various classification techniques. Ghafaryasal *et al.* [5] sequentially applied two different classifiers to remove the FPs based on geometrical information and local image descriptors. Fazlollahi *et al.* [6] utilized a cascade of random forest (RF) classifiers using Radon-based features. Barnes *et al.* [7] used a support vector machine (SVM) classifier with the shape and intensity information. Meanwhile, some other studies also focused on exploring transformations for better representation of CMB regions. Kuijf *et al.* [8] computed the radial symmetry transform to intensify spherical regions on 7.0T Magnetic Resonance (MR) images for CMB detection. Bian *et al.* [9] performed a 2D fast radial symmetry transform to screen initial candidates, followed by geometric feature measurement. However, these methods are limited to intensity-based, geometrical and hand-crafted features which may not be sufficient to encode the complicated spatial information of CMB anatomical structure. Fig. 1 illustrates the spatial information which helps to distinguish CMBs from CMB mimics during the rating procedure.

In this paper, we propose an automatic computer-aided system for CMB detection from brain SWI images, which takes advantage of the compact 3D hierarchical features learned from a stacked convolutional Independent Subspace Analysis (ISA) network. Different from previous methods, our features are learned from the ISA network in an unsupervised way, which helps to explore the underlying discriminative characteristics of CMB regions with limited training data. We validated the representation capability of the learned hierarchical features on the test dataset containing 19 subjects with 161 CMBs. Experimental results achieved

978-1-4244-9270-1/15/$31.00 ©2015 IEEE

a high sensitivity of 89.44% with an average of 7.7 and 0.9 FPs per subject and per CMB, respectively.

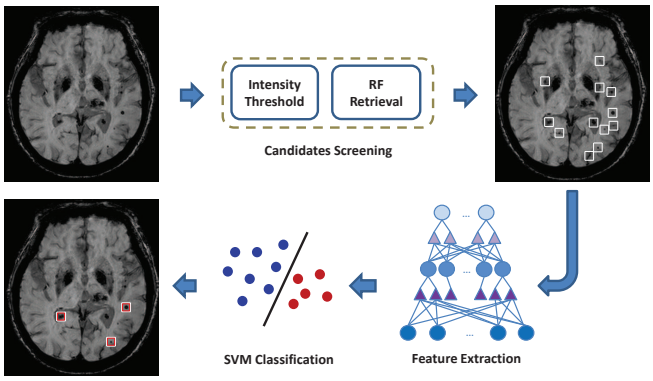

Fig. 2. The overview of the proposed approach for CMB detection. (White and red rectangles denote candidates and detected true CMBs, respectively.)

II. Method

The proposed automatic computer-aided CMB detection system consists of three stages: candidates screening, hierarchical features extraction, and SVM classification with the learned features (as shown in Fig. 2). In the first stage, initial candidate regions are screened based on intensity information. In the second stage, 3D hierarchical feature representations of the candidate cubic regions are extracted from an unsupervised stacked convolutional ISA network. Finally, a SVM classifier is utilized to identify the true CMBs based on the previously learned compact features.

A. Candidates Screening

The candidates screening stage includes two steps: initial candidates selection with intensity thresholding and candidates retrieval with a RF classifier. In the first step, we generate a binary mask by globally thresholding the intensity values to detect hypointense regions in the image. Here we remove the impractically tiny or large regions by restricting the volume size of the connected regions. In the second step, a binary RF classifier is utilized to screen the previously obtained candidates. The RF classifier is trained based on the input of raw intensity values. As a result, this stage can efficiently remove a large number of non-microbleed regions, leaving the false positive candidates which can not be easily identified relying only on low level features.

B. 3D Hierarchical Feature Extraction with ISA Network

Assuming that the sampled 3D image patches construct a feature space, we aim to extract the discriminative characteristics of the microbleed and non-microbleed regions for CMB identification. Considering limited available data tend to cause overfitting and degrade the performance of supervised learning methods, we utilize the unsupervised learning algorithm of ISA which extracts invariant features for object detection by exploring the underlying subspace structure of the data [10].

Specifically, the n-th $(n = 1, ..., N)$ sample is denoted as a 3D volume $v_n \in \mathbb{R}^{d_1 \times d_2 \times d_3}$ centering at O_n. The volume

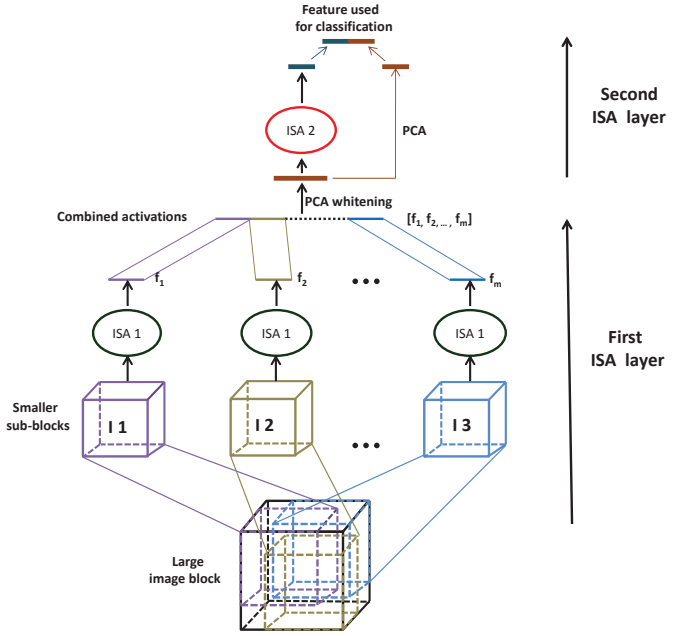

Fig. 3. The stacked convolutional ISA architecture.

v_n is then reshaped into the input vector x_n. Given a basis filter w_i $(i = 1, ..., I)$, the activation is represented as $w_i \cdot x_n$. In ISA, several similar filters are grouped together to span a subspace. Filters of different subspaces are restricted to be independent whereas filters within each subspace are not necessarily independent. Suppose that we aim to extract K dimensional features. Let us denote S_k $(k = 1, ..., K)$ as the set of linear detectors that belong to the k-th subspace, e.g., $S_1 = \{w_1, w_2\}$ means that filters w_1 and w_2 span the first subspace. By introducing a non-linear function, each subspace can generate one invariant feature and the activation of the k-th subspace is represented as:

$$p_k = \sqrt{\sum_{w_i \in S_k} (w_i \cdot x_n)^2} \tag{1}$$

Denoting the subspace structure of the ISA by the matrix $V = [v_{ik}]_{i=1,...,I,k=1,...K}$, where each entry $v_{ik} \in \{0, 1\}$ represents whether the filter w_i is included in the k-th subspace, and denoting the filters matrix by $W = [w_1, ..., w_I]$, ISA is formulated as the following optimization problem:

$$\min \sum_{n=1}^{N} \sum_{k=1}^{K} p_k(x_n; W, V), \quad \text{s.t. } WW^{\mathrm{T}} = I. \tag{2}$$

In order to extract compact hierarchical features for CMB detection, we apply the two-layer ISA network [11] which borrows the concepts of convolution and stacking from deep learning techniques. The stacked ISA architecture is shown in Fig. 3. We initially sample relatively large image blocks. A sliding box is then utilized to obtain overlapping smaller subsamples which are forwarded to the 1st layer ISA. Next, the responses of the subsamples are concatenated as the input to the 2nd layer to extract hierarchical representations. In order to efficiently train ISA, all the input vectors are

pre-processed by principal component analysis (PCA) for dimension reduction. As a result, compact 3D hierarchical features are efficiently extracted from cubic regions in an unsupervised way.

C. Classification with Compact 3D Features

The large number of false positive candidates generated by the RF classifier are further removed by taking advantage of the compact features learned from the ISA network. The 3D hierarchical feature vector r_n is forwarded to the SVM [12] classifier, as shown in Eq. 3.

$$\arg\min_{w} ||w||_2^2 + \alpha \sum_{n=1}^{N} \max(0, 1 - y_n w^{\mathrm{T}} r_n) \qquad (3)$$

where $y_n \in \{+1, -1\}$ is the label of the sample x_n and α controls the tradeoff between the weight decay term and the hinge loss term.

III. Experiments and Results

A. Dataset

Our dataset contains 44 patients with 25 subjects for training and 19 subjects for testing. For each subject, a SWI MR scan was performed on a 3.0T Philips Medical System with a 3D spoiled gradient-echo sequence. Each image was acquired with the parameters set as 0.45×0.45 mm^2 in-plane resolution, 2 *mm* slice thickness, 1 *mm* slice spacing, and a 230×230 mm^2 field of view. Microbleeds in the SWI volumes were visually rated by two experienced neuroradiologists independently according to the standard of Microbleed Anatomical Rating Scale [13]. A total of 615 CMBs (454 for training and 161 for testing) were manually annotated as the ground truth in our experiments. The intensity range of the image was normalized to $[0, 1]$ during the preprocessing procedure.

B. Experiments

In the candidates screening stage, the parameters were determined on the training dataset based on the analysis of intensity distribution of the microbleed regions. When training the RF classifier, additional positive samples were augmented by rotation and translation. Meanwhile, non-CMB regions were randomly sampled from the whole brain images. In the hierarchical features extraction stage, ISA training samples were extracted from the whole dataset (both training and testing), taking advantage of the unsupervised property of the ISA network. Given a candidate location, an image block of size $20 \times 20 \times 14$ was sampled as the input and the convolution stride was set to 4 in each direction. The subspace size was set to 2 and the ISA network finally extracted 200 features by combining the activations from hierarchical layers.

C. Qualitative Results

The typical filters learned by the first layer of the ISA network are shown in Fig. 4. There, each column represents a 3D filter which is visualized as 2D filter maps tiled along the third dimension. We can see that the filters can effectively capture the rounded shape of the CMBs. Meanwhile, edge detectors with various frequencies and orientations are also learned from the ISA network.

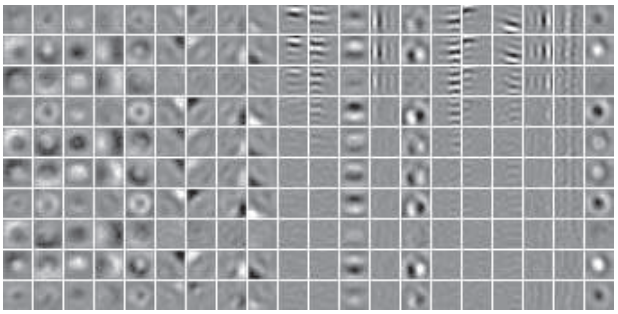

Fig. 4. The typical learned filters of the 1st layer ISA.

In addition, the feature representations extracted from the stacked ISA network are visualized by projecting them onto a 2D plane using the t-SNE method [14]. As shown in Fig. 5, the CMB samples and non-CMB samples are well separated, which demonstrates the representation capability of the compact 3D hierarchical features. Typical detection results are illustrated in Fig. 6, which proves the effectiveness of our method to identify CMBs.

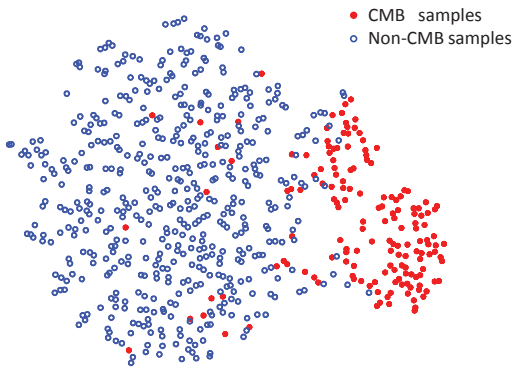

Fig. 5. 2D t-SNE embedding of ISA features. (Red dots and blue circles are CMB and non-CMB samples, respectively.)

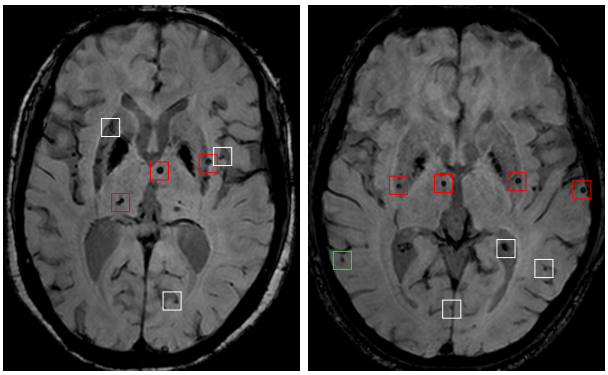

Fig. 6. Examples of detection results: detected true CMBs (red rectangle), removed false candidates (white rectangle), and FP (green rectangle).

D. Quantitative Evaluation

We quantitatively evaluated the performance of our approach with the following 4 metrics: recall (R), precision (P), number of FPs per subject (FPs/sub) and number of FPs per CMB (FPs/CMB), which are defined as below:

$$\begin{aligned} \mathrm{R} &= \frac{TP}{TP+FN}, \quad \mathrm{P} = \frac{TP}{TP+FP}, \\ \mathrm{FPs/sub} &= \frac{FP}{M}, \quad \mathrm{FPs/CMB} = \frac{FP}{TP+FN}. \end{aligned} \tag{4}$$

where TP, FP and FN denote the number of true-positive, false-positive and false-negative detection results, respectively. M is the number of testing subjects.

The parameters of the candidates screening stage were set to preserve a high sensitivity (recall) during experiments. As shown in Table I, the number of FPs are significantly reduced throughout the pipeline. The final detection performance achieved a recall of 89.44% with an average of 7.7 FPs per subject. Fig. 7 is the free-response receiver operating characteristic (FROC) curve which describes how the detection sensitivity changes with the number of FPs. Generally, our approach can detect CMBs from one patient within 40 seconds using a PC with a 3.20 GHz Inter(R) i5-4570 CPU.

We compared our proposed approach with the previously reported methods in Table II. Since the subjects containing more CMBs tend to get more FPs, we utilized the metric of FPs/CMB, which is not as sensitive to the various datasets as FPs/sub, for a relatively fair comparison [9]. Results showed that our algorithm outperformed the other methods by a large margin with only an average of 0.9 FPs per CMB while preserving a high sensitivity.

TABLE I
EXPERIMENTAL RESULTS

Steps	Recall	Precision	FPs/sub	FPs/CMB
Thresholding	1	0.0105	807	95
RF retrieval	0.9441	0.0403	190	23
SVM classification	0.8944	0.4966	7.7	0.9

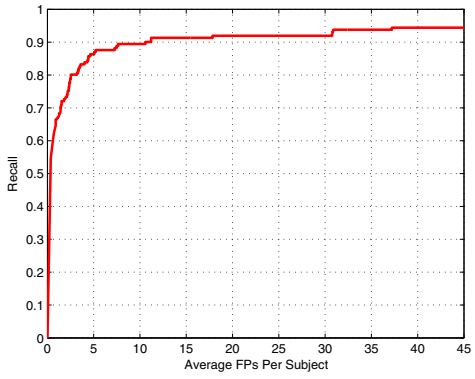

Fig. 7. FROC curve of our proposed approach.

IV. CONCLUSION

In this paper, we propose a computer-aided system to automatically detect CMBs from brain SWI images with the high sensitivity and low false positive rate. The 3D hierarchical features are extracted from a stacked convolutional ISA network for discriminative classification. Experimental results on the dataset containing 19 elderly subjects (161 CMBs) validated the efficacy of our method.

TABLE II
COMPARISON OF PERFORMANCE AMONG ALGORITHMS

Methods	Recall	FPs/sub	FPs/CMB
Ghafaryasal *et. al* [5]	0.909	**4.1**	1.8
Fazlollahi *et. al* [6]	**0.920**	16.8	6.7
Barnes *et. al* [7]	0.817	107.5	5.4
Kuijf *et. al* [8]	0.712	17.2	4.7
Bian *et. al* [9]	0.865	44.9	1.5
Ours	0.894	7.7	**0.9**

REFERENCES

[1] S. M. Greenberg, M. W. Vernooij, C. Cordonnier, A. Viswanathan, R. Al-Shahi Salman, S. Warach, L. J. Launer, M. A. Van Buchem, and M. Breteler, "Cerebral microbleeds: a guide to detection and interpretation," *The Lancet Neurology*, vol. 8, no. 2, pp. 165–174, 2009.

[2] A. Charidimou, A. Krishnan, D. J. Werring, and H. R. Jäger, "Cerebral microbleeds: a guide to detection and clinical relevance in different disease settings," *Neuroradiology*, vol. 55, no. 6, pp. 655–674, 2013.

[3] J. de Bresser, M. Brundel, M. Conijn, J. van Dillen, M. Geerlings, M. Viergever, P. Luijten, and G. Biessels, "Visual cerebral microbleed detection on 7t mr imaging: reliability and effects of image processing," *American Journal of Neuroradiology*, vol. 34, no. 6, pp. E61–E64, 2013.

[4] A. Charidimou and D. J. Werring, "Cerebral microbleeds: detection, mechanisms and clinical challenges," *Future Neurology*, vol. 6, no. 5, pp. 587–611, 2011.

[5] B. Ghafaryasl, F. van der Lijn, M. Poels, H. Vrooman, M. A. Ikram, W. J. Niessen, A. van der Lugt, M. Vernooij, and M. de Bruijne, "A computer aided detection system for cerebral microbleeds in brain mri," in *Biomedical Imaging (ISBI), 2012 9th IEEE International Symposium on*. IEEE, 2012, pp. 138–141.

[6] A. Fazlollahi, F. Meriaudeau, V. L. Villemagne, C. Rowe, P. Yates, O. Salvado, P. T. Bourgeat *et al.*, "Efficient machine learning framework for computer-aided detection of cerebral microbleeds using the radon transform," in *Proceedings of the IEEE-ISBI conference*, 2014.

[7] S. R. Barnes, E. M. Haacke, M. Ayaz, A. S. Boikov, W. Kirsch, and D. Kido, "Semiautomated detection of cerebral microbleeds in magnetic resonance images," *Magnetic resonance imaging*, vol. 29, no. 6, pp. 844–852, 2011.

[8] H. J. Kuijf, J. de Bresser, M. I. Geerlings, M. Conijn, M. A. Viergever, G. J. Biessels, and K. L. Vincken, "Efficient detection of cerebral microbleeds on 7.0 t mr images using the radial symmetry transform," *NeuroImage*, vol. 59, no. 3, pp. 2266–2273, 2012.

[9] W. Bian, C. P. Hess, S. M. Chang, S. J. Nelson, and J. M. Lupo, "Computer-aided detection of radiation-induced cerebral microbleeds on susceptibility-weighted mr images," *NeuroImage: clinical*, vol. 2, pp. 282–290, 2013.

[10] A. Hyvärinen, J. Hurri, and P. O. Hoyer, *Natural Image Statistics: A Probabilistic Approach to Early Computational Vision.* Springer Science & Business Media, 2009, vol. 39.

[11] Q. V. Le, W. Y. Zou, S. Y. Yeung, and A. Y. Ng, "Learning hierarchical invariant spatio-temporal features for action recognition with independent subspace analysis," in *Computer Vision and Pattern Recognition (CVPR), 2011 IEEE Conference on*. IEEE, 2011, pp. 3361–3368.

[12] C.-C. Chang and C.-J. Lin, "Libsvm: a library for support vector machines," *ACM Transactions on Intelligent Systems and Technology (TIST)*, vol. 2, no. 3, p. 27, 2011.

[13] S. Gregoire, U. Chaudhary, M. Brown, T. Yousry, C. Kallis, H. Jäger, and D. Werring, "The microbleed anatomical rating scale (mars) reliability of a tool to map brain microbleeds," *Neurology*, vol. 73, no. 21, pp. 1759–1766, 2009.

[14] L. Van der Maaten and G. Hinton, "Visualizing data using t-sne," *Journal of Machine Learning Research*, vol. 9, no. 2579-2605, p. 85, 2008.